DALTON

Mono- and di-nuclear complexes of molybdenum carbonyl derivatives with pyridine-2-carbaldehyde azine and phosphines: syntheses, structure, spectroscopic and electrochemical characterisation and solvatochromic effects†

Juan Granifo,*[a] Moisés E. Vargas,[a] Elaine S. Dodsworth,*[b] David H. Farrar,[c] Scott S. Fielder[b] and A. B. P. Lever[b]

[a] *Departamento de Ciencias Químicas, Universidad de La Frontera, Casilla 54-D, Temuco, Chile*
[b] *Department of Chemistry, York University, North York, Ontario, Canada M3J 1P3*
[c] *Department of Chemistry, University of Toronto, Toronto, Ontario, Canada M5S 3H6*

Complexes containing phosphorus-donor ligands, $[Mo(CO)_3(PPh_3)(pa)]$ (pa = pyridine-2-carbaldehyde azine), $[Mo_2(CO)_6(PPh_3)_2(\mu\text{-pa})]$, $[Mo_2(CO)_7(PPh_3)(\mu\text{-pa})]$ and $[Mo_2(CO)_6(\mu\text{-dppe})(\mu\text{-pa})]$ [dppe = 1,2-bis(diphenylphosphino)ethane], have been characterised by infrared and electronic spectroscopy, cyclic voltammetry and for the $[Mo_2(CO)_6(\mu\text{-dppe})(\mu\text{-pa})]$ complex a single crystal X-ray structure. All of the complexes show strong solvatochromism which has been analysed both by using the empirical parameter E^*_{MLCT} and by using McRae's equation. The results are compared with those of their parent complexes $[Mo(CO)_4(pa)]$ and $[Mo_2(CO)_8(\mu\text{-pa})]$, and with the results of extended-Hückel calculations with charge iteration.

Polynuclear complexes involving chelating polypyridyl ligands have been of increasing interest recently,[1] and a number of molybdenum and tungsten carbonyl derivatives have been studied.[2-6] The nature of the bridging ligand, in these multimetallic complexes, has a significant influence upon the communication between the metal centres.[7] In the case of a weak interaction the properties of the polynuclear complexes are simply the addition of their molecular components. In the case of strong interaction, the properties are different when compared with those of the mononuclear components. In a series of ligands reported by Haga and Koizumi[6] pyridine-2-carbaldehyde azine (pa) was found to have a strong interaction between the two ends of the ligand; it was therefore expected to facilitate interaction between the two metals in the $[Mo(CO)_4]$ derivatives.

We report here the behaviour of this system when CO groups are replaced by phosphines, which make the metal more electron-rich so that it should interact more strongly with the bridging ligand π^* system[4c,5e,8] and might also interact more strongly with the second metal in the dinuclear species. For comparison with the respective mononuclear parent complexes we have also prepared the new tetracarbonyl complex $[Mo(CO)_4(pa)]$. Thus, the triphenylphosphine complexes $[Mo(CO)_3(PPh_3)(pa)]$ (mononuclear), $[Mo_2(CO)_6(PPh_3)_2(\mu\text{-pa})]$ (symmetric dinuclear) and $[Mo_2(CO)_7(PPh_3)(\mu\text{-pa})]$ (asymmetric dinuclear) have been isolated and investigated by spectroscopic and electrochemical methods. In addition, the diphosphine-bridged compound of formula $[Mo_2(CO)_6(\mu\text{-dppe})(\mu\text{-pa})]$ [dppe = 1,2-bis(diphenylphosphino)ethane] has been isolated; the crystal structure of this species shows a dinuclear complex with an intramolecular dppe bridge and thus a more rigid structure than the analogous $[Mo_2(CO)_6(PPh_3)_2(\mu\text{-pa})]$ complex. The electronic structures of all these species have been modelled by using extended-Hückel molecular orbital (EHMO) theory with charge iteration. We were interested to know how well this theory would model the behaviour of this type of complex.

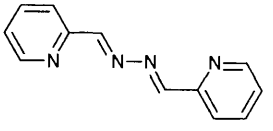

pa

These complexes are also of interest from the point of view of their solvatochromic behaviour.[9-12] The dinuclear species contain two dipoles which may, in principle, be parallel, antiparallel, orthogonal, or somewhere in between (subject to steric constraints). We have previously discussed the question of whether the two halves of such a dinuclear species interact essentially independently with the solvent and whether the excited state is localised on one or both metals *etc.*[9] The data presented here help to clarify some of these issues.

Experimental

Preparation of complexes

All the reactions were carried out under nitrogen and with deaerated solvents. The compounds $[Mo(CO)_6]$, PPh_3 and $Ph_2PCH_2CH_2PPh_2$ (dppe) were purchased from Aldrich Chemical Co. Pyridine-2-carbaldehyde azine,[13] $[Mo(CO)_4(pip)_2]$ (pip = piperidine)[14] and $[Mo_2(CO)_8(\mu\text{-pa})]$[6] were obtained following similar methods to those described in the literature. The complexes, $[Mo(CO)_3(NCMe)(pa)]$ and $[Mo_2(CO)_6(NCMe)_2(\mu\text{-pa})]$ were isolated according to the procedure described in the literature[15] for preparing acetonitrile derivatives by refluxing $[Mo(CO)_4(pa)]$ or $[Mo_2(CO)_8(\mu\text{-pa})]$ in MeCN for 2 h.

$[Mo(CO)_4(pa)]$. A mixture of pyridine-2-carbaldehyde azine

† *Supplementary data available* (No. SUP 57177, 3 pp.): electronic absorption maxima of the molybdenum pyridine-2-carbaldehyde azine complexes in various solvents. See Instructions for Authors, *J. Chem. Soc., Dalton Trans.*, 1996, Issue 1.

Non-SI unit employed: eV ≈ 1.60 × 10^{-19} J.

Table 1 Analytical and IR spectroscopic data for the molybdenum pyridine-2-carbaldehyde azine complexes

Compound	Analysis[a] (%)			IR[b]/cm^{-1}
	C	H	N	ν(C≡O)
$[Mo(CO)_4(pa)]$	45.3 (46.0)	2.4 (2.4)	13.5 (13.4)	2005, 1915, 1875, 1820
$[Mo(CO)_3(PPh_3)(pa)]$	60.1 (60.7)	3.7 (3.9)	8.8 (8.6)	1910, 1825, 1790
$[Mo_2(CO)_6(PPh_3)_2(\mu\text{-pa})]$	58.9 (59.2)	3.7 (3.7)	5.4 (5.1)	1910, 1830, 1795
$[Mo_2(CO)_6(\mu\text{-dppe})(\mu\text{-pa})]\cdot 0.6CH_2Cl_2$	52.2 (52.5)	3.5 (3.5)	5.5 (5.5)	1915, 1830, 1795
$[Mo_2(CO)_7(PPh_3)(\mu\text{-pa})]$	52.0 (52.7)	2.8 (2.9)	6.6 (6.5)	2010, 1920, 1880, 1825, 1790

[a] Required values are given in parentheses. [b] As KBr discs.

(1.18 g, 5.6 mmol) and $[Mo(CO)_4(pip)_2]$ (1.77 g, 4.7 mmol) in diethyl ether (100 cm^3) was stirred overnight. The resulting purple solution with a dark precipitate {mainly $[Mo(CO)_4(pa)]$ and $[Mo_2(CO)_8(\mu\text{-pa})]$} was filtered and the solid was washed twice with 10 cm^3 portions of diethyl ether. The complex $[Mo(CO)_4(pa)]$ was obtained by soxhlet extraction with diethyl ether for 5 h. The crystalline dark brown $[Mo(CO)_4(pa)]$ was filtered off and washed with diethyl ether. Yield 0.44 g (22%).

$[Mo(CO)_3(PPh_3)(pa)]$, $[Mo_2(CO)_6(PPh_3)_2(\mu\text{-pa})]$ and $[Mo_2(CO)_6(\mu\text{-dppe})(\mu\text{-pa})]$. These complexes were prepared by similar methods from fresh samples of the above acetonitrile derivatives. The following procedure is typical.

$[Mo_2(CO)_6(\mu\text{-dppe})(\mu\text{-pa})]\cdot 0.6CH_2Cl_2$. To a solution of freshly prepared $[Mo_2(CO)_6(NCMe)_2(\mu\text{-pa})]$ (0.26 g, 0.40 mmol) in CH_2Cl_2 (90 cm^3) was added dppe (0.159 g, 0.40 mmol) and the mixture was stirred for 2 h. The dark green solution was then filtered, 45 cm^3 of MeOH were added to the filtrate and the solution was refrigerated overnight. Dark green crystals were separated by filtration, washed with three portions of MeOH (10 cm^3) and dried *in vacuo*. Yield 0.30 g (74%).

$[Mo_2(CO)_7(PPh_3)(\mu\text{-pa})]$. To a solution of $[Mo(CO)_3(PPh_3)(pa)]$ (0.125 g, 0.019 mmol) in CH_2Cl_2 (10 cm^3) was added $[Mo(CO)_4(pip)_2]$ (0.073 g, 0.019 mmol). The green-blue solution was stirred for 1 h, filtered and evaporated to dryness. The solid was washed three times with hot MeOH (10 cm^3) and the black residue was dissolved in CH_2Cl_2 (10 cm^3) and the solution filtered. Upon addition of petroleum ether (b.p. 40–60 °C, 50 cm^3) black crystals formed. Yield 0.05 g (30%).

Elemental analyses of all compounds isolated are presented in Table 1.

Instrumentation

Infrared spectra were recorded on a Perkin-Elmer 577 spectrophotometer, and electronic spectra on a Spectronic 3000 or HP 8452 diode array spectrophotometer or a Varian-Cary 2400. Cyclic voltammograms were obtained in dimethylformamide (dmf) containing tetrabutylammonium hexafluorophosphate (0.1 mol dm^{-3}) as supporting electrolyte. Three-electrode measurements were carried out with a RDE 3 potentiostat (Pine Instruments) and an X-Y recorder. A platinum-disc working electrode, platinum wire auxiliary electrode and a AgCl–Ag reference electrode [with internal reference ferrocenium–ferrocene, 0.493 V *vs.* saturated calomel electrode (SCE) in dmf[16]] were used in the cyclic voltammetry experiments.

Theoretical methods

Electronic structure calculations were performed at the extended-Hückel or semiempirical levels on a Silicon Graphics 4D/35 or R4000 Indigo computer. Semiempirical AM1 calculations were performed using the SPARTAN 3.1 system of programs (Wavefunction Inc., Irvine, CA). Constrained optimisations were carried out using the method of Baker.[17] Geometry optimisations at the AM1 level used a BF_2^+ fragment to mimic the effect of the metal.[18] It was necessary to constrain the B–N distances to prevent the boron from being three-co-ordinate. Extended-Hückel calculations with charge iteration[19] and oscillator strength calculations[20,21] were carried out using in-house code, with parameters from Vela and Gazquez,[22] from geometries obtained from the SPARTAN molecular mechanics routine. Our method[21] of calculating oscillator strengths differs slightly from that of Calzaferri and Rytz.[20] The Mo–CO distances were constrained to be 1.94 Å (Mo–N and Mo–P obtained from SPARTAN agree well with the crystal structure data) and dihedral angles were constrained where necessary. Methyl groups were used instead of phenyl rings in the dppe and PPh_3 model complexes to simplify the structures.

Crystal-structure determination of $[Mo_2(CO)_6(\mu\text{-dppe})(\mu\text{-pa})]\cdot 0.6CH_2Cl_2$.

Dark green crystals of $C_{44}H_{34}Mo_2N_4O_6P_2\cdot 0.6CH_2Cl_2$, were grown from CH_2Cl_2–MeOH by slow cooling. A malformed dihedron of approximate dimensions 0.17 × 0.18 × 0.45 mm was mounted on a glass fibre.

Crystal data. $C_{44}H_{34}Mo_2N_4O_6P_2\cdot 0.6CH_2Cl_2$, M = 1019.56, monoclinic, space group $C2/c$, a = 23.017(5), b = 12.219(4), c = 17.292(4) Å, β = 95.15(2)°, U = 4844(2) Å^3, Z = 4, D_x = 1.40 g cm^{-3}, T = 25 °C, λ(Mo-Kα) = 0.710 73 Å, μ(Mo-Kα) = 0.70 mm^{-1}, $F(000)$ = 2052.8.

Data collection and processing. Accurate cell dimensions and crystal orientation matrix were determined on a CAD-4 diffractometer by a least-squares treatment of the setting angles of 25 reflections in the range $14 < \theta < 29°$. Intensities of reflections with indices h −24 to 24, k 0–13, l 0–18 with $1 < \theta < 22.5°$ measured, ω–2θ scans, ω scan width (0.9 + 0.35 tan θ)°; graphite-monochromatised Mo-Kα radiation; intensities of three reflections measured every 2 h showed an average decrease of 15.6%. The 3158 reflections measured were corrected for Lorentz and polarisation effects. Data were corrected for decay. Crystal faces were identified as the forms {110} and {001}. 2948 Data with $I > 3\sigma(I)$ were labelled, observed and used in the structure solution and refinement. Due to the malformed nature of the crystal, the data were corrected for absorption by the program DIFABS (minimum, maximum correction 0.851/1.091).[23] This correction lowered the R factor by approximately 0.01 and slightly improved the Mo and P thermal parameters.

Structure analysis and refinement. An examination of the statistics associated with the intensities suggested that the space group was centrosymmetric. The space group $C2/c$ was determined by the systematic absences (hkl absent if $h + k = 2n + 1$, $h0l$ absent if $l = 2n + 1$) and by a successful structure solution and refinement. The structure was solved by the heavy atom method. Refinement was by full-matrix least-squares calculations on F, initially with isotropic and then with anisotropic

Table 2 Selected bond lengths (Å) and angles (°) for $[Mo_2(CO)_6(\mu\text{-dppe})(\mu\text{-pa})]\cdot 0.6CH_2Cl_2$ with estimated standard deviations in parentheses

Mo–C(1)	1.927(7)	Mo–C(2)	1.939(7)
Mo–C(3)	1.972(7)	Mo–N(1)	2.255(5)
Mo–N(2)	2.239(5)	Mo–P	2.5347(18)
C(2)–Mo–C(1)	87.96(30)	C(3)–Mo–C(1)	85.87(30)
N(1)–Mo–C(1)	100.97(25)	N(2)–Mo–C(1)	172.82(25)
P–Mo–C(1)	93.04(23)	C(3)–Mo–C(2)	87.58(30)
N(1)–Mo–C(2)	170.90(24)	N(2)–Mo–C(2)	99.20(24)
P–Mo–C(2)	88.38(23)	N(1)–Mo–C(3)	94.76(23)
N(2)–Mo–C(3)	94.82(24)	P–Mo–C(3)	175.84(20)
N(2)–Mo–N(1)	71.86(18)	P–Mo–N(1)	89.39(14)
P–Mo–N(2)	86.77(14)	C(11)–N(1)–Mo	118.0(4)
C(12)–N(2)–Mo	116.8(4)	C(12)–C(11)–N(1)	117.4(6)
N(2)–C(12)–C(11)	115.8(6)	C(4)–P–Mo	114.03(22)
C(4')–C(4)–P	110.2(3)		

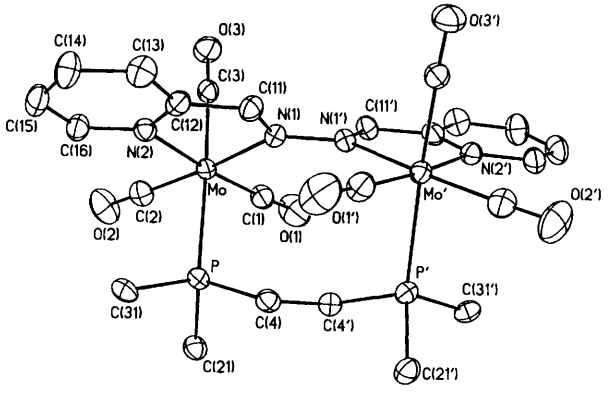

Fig. 1 Perspective view of the $[Mo_2(CO)_6(\mu\text{-dppe})(\mu\text{-pa})]$ complex showing the atom numbering scheme. Phenyl rings are omitted for clarity. 25% Probability ellipsoids are shown

thermal parameters. The lattice also contains a disordered molecule of CH_2Cl_2. The major orientation of the solvent molecule refined to an occupancy factor of 0.5 with three other orientations at a total site occupancy of 0.1. In the final rounds of calculations the hydrogen atoms were positioned on geometric grounds (C–H 0.95 Å) and included (as riding atoms) in the structure factor calculation. These atoms were assigned general isotropic thermal parameters; U_{iso} 0.07 Å^2. The final cycle of refinement included 301 variable parameters, $R = 0.051$, $R' = 0.057$, goodness of fit 3.89, $w = 1/[\sigma^2(F_o) + 0.000\,08(F_o)^2]$. Maximum shift/e.s.d in final refinement cycle 0.07; density in the final difference map in the range −0.59 to 0.80 e Å^{-3}; the largest peak at position (0.4148, 0.2479, 0.1644) was associated with the disordered solvent molecule. No correction was made for secondary extinction. Selected bond distances and angles are given in Table 2. All calculations were carried out on an Apollo computer using SHELX 76 and SHELX 86.[24]

Complete atomic coordinates, thermal parameters, and bond lengths and angles have been deposited at the Cambridge Crystallographic Data Centre (CCDC). See Instructions for Authors *J. Chem. Soc., Dalton Trans.* Issue 1, 1996. Any request to the CCDC for this material should quote the full literature citation and the reference number 186/247.

Results and Discussion

The new compounds isolated in this work (Table 1) are dark blue or green crystalline solids, which are air-stable and soluble in common organic solvents.

Crystal structure of $[Mo_2(CO)_6(\mu\text{-dppe})(\mu\text{-pa})]\cdot 0.6CH_2Cl_2$

A diagram of the structure of the dinuclear complex $[Mo_2(CO)_6(\mu\text{-dppe})(\mu\text{-pa})]$ is shown in Fig. 1. The structure consists of a double bridge bonding the two metal centres. The pa ligand is not planar [dihedral angle C(11),N(1),N(1'), C(11'), is −141(1)°] due to the shortness of the P–C(4)–C(4')–P' chain of the dppe ligand linking the metal atoms. The ligand is closer to the *trans* than to the *cis* configuration. The co-ordination around the molybdenum atoms is distorted octahedral, as is typical for this type of system.[25] The distortion is produced by the five-membered ring of the bonded pa ligand in which the N(1)–Mo–N(2) angle is only 71.86(18)°. The Mo–P distance of 2.5347(18) Å is in the range expected for complexes involving molybdenum carbonyl derivatives and diphosphines[26] and is comparable to a mean value of 2.52(6) Å obtained for the 1606 Mo–P(phosphine) distances reported in the Cambridge Structural Database.[27] The two Mo–N bonds, 2.255(5) and 2.239(5) Å, are chemically different but statistically equivalent. The distances associated with the three Mo–C≡O groups are statistically indistinguishable and comparable to other molybdenum carbonyl derivatives.[26] The bond angles and lengths in the ligands do not vary greatly from expected values.[28]

Infrared spectra

The carbonyl stretching frequencies of the new compounds are given in Table 1. The bands of the monometallic complex $[Mo(CO)_4(pa)]$ are typical of $[Mo(CO)_4(diimine)]$ species.[29] The $[Mo(CO)_3(PPh_3)(pa)]$, $[Mo_2(CO)_6(PPh_3)_2(\mu\text{-pa})]$ and $[Mo_2(CO)_6(\mu\text{-dppe})(\mu\text{-pa})]$ complexes show similar ν(CO) absorptions which reveal the facial conformations of their CO groups.[30] In the asymmetric dinuclear complex, $[Mo_2(CO)_7(PPh_3)(\mu\text{-pa})]$, the five bands are probably due to the superposition of the bands of the *cis* and *fac* structure of its carbonyl groups.

Theoretical results

AM1 Calculations were carried out on pyridine-2-carbaldehyde azine and the mono- and di-nuclear BF_2^+ complexes in order to find the lowest energy conformations of the ligand prior to using the EHMO method for two model complexes. The BF_2^+ group has been used previously to mimic the net electron withdrawing effect of co-ordinating a metal fragment to a ligand.[18]

The azine has a lowest energy conformation with a dihedral angle, C(11),N(1),N(1'),C(11'), of 102° in the centre, and neither end is planar; the pyridine rings are twisted out of the plane of the central part of the ligand by about 50°. Therefore pa cannot be described as either *cis* or *trans*, though it is closer to the *trans* configuration. When BF_2^+ is co-ordinated both the mono- and di-nuclear species are essentially planar (and *trans*) after performing a geometry optimisation (with B–N distances constrained) at the AM1 level. The choice of B–N distances did not affect the results qualitatively. Thus we will assume pa to be planar in all complexes except the dppe-bridged species. This assumption is consistent with the spectroscopic data (see below).

Extended-Hückel molecular orbital calculations have been carried out for mono- and di-nuclear $[Mo(CO)_4]$ complexes, PMe_3-substituted species to model the PPh_3 complexes, and a dppe-bridged model (using $Me_2PCH_2CH_2PMe_2$, dmpe, in place of dppe). The results (metal–ligand interactions, energies and transition intensities) are similar for the carbonyl and phosphine-substituted species. Calculated orbital energies and percentage composition data are given in Tables 3 and 4.

Both AM1 (BF_2^+ complex) and extended-Hückel (Mo complexes) calculations show the lowest unoccupied molecular

Table 3 Calculated energies of the valence orbitals[a]

Mononuclear complexes

	HOMO-2	HOMO-1	HOMO	LUMO	LUMO+1
$[Mo(CO)_4(pa)]$	−11.03[b]	−10.99[b]	−10.63	−10.07	−9.07
$[Mo(CO)_3(PMe_3)(pa)]$	−10.18	−10.12	−10.09	−9.74	−8.89

Dinuclear complexes

	HOMO-5	HOMO-4	HOMO-3	HOMO-2	HOMO-1	HOMO	LUMO	LUMO+1
$[Mo_2(CO)_8(\mu\text{-pa})]$	−11.07	−11.065	−11.03	−11.02	−10.68	−10.63	−10.31	−9.46
$[Mo_2(CO)_6(PMe_3)_2(\mu\text{-pa})]$[c]	−10.21	−10.16	−10.12	−10.11	−10.08	−10.06	−9.79	−9.05
$[Mo_2(CO)_6(\mu\text{-L})(\mu\text{-pa})]$[d]	−10.23	−10.17	−10.13	−10.11	−10.09	−10.03	−9.67	−9.09
$[Mo_2(CO)_7(PMe_3)(\mu\text{-pa})]$	−11.02[e]	−10.99[e]	−10.62[e]	−10.30[f]	−10.23[f]	−10.19[f]	−10.03	−9.21

[a] Energies are given in eV. [b] The pyridine-based σ orbital that is calculated to be the HOMO-1 in $[Mo(CO)_4(pa)]$ has been omitted to avoid confusion since it lies below the Mo dπ levels in all the other complexes. [c] Data given for C_i symmetry isomer, energies for C_2 isomer are the same within ±0.01 eV. [d] L = dmpe or dppe. [e] Orbital localised on $[Mo(CO)_4]$ end of the complex. [f] Orbital localised on $[Mo(CO)_3(PMe_3)]$ end of the complex.

Table 4 Calculated percentage composition of the valence orbitals[a]

Complex	HOMO-5	HOMO-4	HOMO-3	HOMO-2	HOMO-1	HOMO	LUMO	LUMO+1
$[Mo(CO)_4(pa)]$				40.3[b]	41.7[b]	48.3	1.0	0.1
				7.3	3.2	3.3	96.1	98.5
$[Mo(CO)_3(PMe_3)(pa)]$				38.0	46.7	47.4	7.0	0.9
				25.0	3.2	2.6	84.1	96.5
$[Mo_2(CO)_8(\mu\text{-pa})]$	41.1	39.8[c]	41.9	42.5	48.3	48.8	1.7	0.5
	6.0	8.6	3.6	2.4	2.3	3.4	94.4	95.9
$[Mo_2(CO)_6(PMe_3)_2(\mu\text{-pa})]$[d]	33.3	44.6	47.1	47.1	47.3	47.4	11.9	2.4
	33.8	11.3	2.1	3.5	2.6	3.1	73.6	91.6
$[Mo_2(CO)_6(\mu\text{-L})(\mu\text{-pa})]$[e]	34.4	45.1	47.0	47.3	47.6	44.0	12.4	2.8
	30.6	10.5	4.5	2.0	2.8	6.0	72.6	90.3
$[Mo_2(CO)_7(PMe_3)(\mu\text{-pa})]$	40.7[f]	42.0[f]	48.3[f]	36.5[g]	47.5[g]	47.6[g]	8.3	1.7
	6.3[f]	3.2[f]	3.0[f]	27.6[g]	3.0[g]	2.8[g]	81.4	93.3

[a] For each complex the first line contains the percentage Mo and the second line the percentage pa. [b] The pyridine-based σ orbital that is calculated to be the HOMO-1 in the $[Mo(CO)_4(pa)]$ complex has been omitted as in Table 3. [c] This orbital is the in-phase combination of Mo d_{yz} orbitals, which always has the lowest percentage Mo since it mixes most strongly with the pa ligand-based LUMO; in the other complexes the in-phase combination lies lowest. [d] Data given for C_i symmetry isomer, percentages for C_2 isomer are the same within ±0.2%. [e] L = dmpe. [f] Orbital localised on $[Mo(CO)_4]$ end of the complex. [g] Orbital localised on $[Mo(CO)_3(PMe_3)]$ end of the complex.

orbital (LUMO) and LUMO+1 in the dinuclear species to be a pair of π* orbitals extending over the whole pa ligand and differing only in the presence or absence of a node bisecting the central N–N bond (Fig. 2). As the central dihedral angle increases the relative energies of these two orbitals change, the LUMO increases and the LUMO+1 decreases in energy and they become a degenerate pair at a dihedral angle of 90°.

Similar results are obtained for the mononuclear complexes. Both the LUMO and LUMO+1 are distributed over the whole ligand when it is flat, though in this case they are not equally spread over both halves because of the presence of the metal. The LUMO increases in energy as the C(11),N(1),N(1′),C(11′) dihedral angle becomes closer to 90°, and at 90° the LUMO is almost entirely localised on the half of the ligand with the Mo co-ordinated. The LUMO and LUMO+1 are not degenerate in this case, though they are close in energy, and the LUMO+1 is largely localised on the unmetallated half of the ligand.

The metal valence orbitals (t_{2g} in O_h symmetry) in the mononuclear species appear like those of a complex with C_{2v} symmetry[12,31] (pa ligand lies in xz plane and C_2, z, axis bisects the N–Mo–N angle). All three orbitals are stabilised by strong π-backbonding to CO π* orbitals (see Fig. 2) and there are much weaker interactions with pa π and π* levels (Table 4). The Mo–pa π mixing is enhanced in the phosphine-substituted species, and in the dinuclear relative to the mononuclear complexes.

We use a d orbital set in which the metal valence (dπ) orbitals are $d_{x^2-z^2}$ and d_{yz} and the unoccupied dσ orbitals are d_{y^2} and d_{xz}. As shown in Fig. 3, the 'a_1' ($d_{x^2-z^2}$) level, which lies in the plane of the pa ligand and overlaps with a pa σ level, is highest, next is the 'a_2' (d_{xy}) which interacts with the pa π system in a 'δ' manner, but is non-bonding with respect to both the LUMO and LUMO+1 of pa, and the lowest of the three is b_2 in $C_{2v}(d_{yz})$ which is stabilised by backbonding to the LUMO. This calculated ordering differs from that published previously for complexes of this type;[9b,31] the d_{xy} is normally placed lower than d_{yz} in spite of its weaker interaction with the diimine ligand. This was probably because for many $[Mo(CO)_4(diimime)]$ complexes the lowest charge-transfer band shows a shoulder to higher energy in non-polar solvents, which was attributed to the transition from d_{xy}, with the main transition being from d_{yz}. However, the ordering of the transitions may not be the same as the ordering of the orbitals because of differences in the vibrational reorganisation energies associated with the transitions, differences in the Coulombic and exchange contributions,[32] and the effects of configuration interaction.

In the dinuclear species the two sets of t_{2g} orbitals combine in- and out-of-phase, with the strength of the interaction depending on the relative orientations of the two d orbitals (Fig. 3, Table 3). The strongest interaction occurs between the $d_{x^2-z^2}$ orbitals which lie in the σ plane of the pyridine-2-carbaldehyde azine ligand. Although the energies obtained from the EHMO method are only a crude approximation, the interaction between the two metals appears to be quite weak as the pairs of in- and out-of-phase combinations have very similar energies. Due to interactions with lower-lying levels the in-phase combination is not always calculated to be the lower of a given pair, particularly in the $[Mo(CO)_4]$ complexes where the dπ levels are lower and closer to the pa π levels. Some of the molecular orbital surfaces are shown in Fig. 2.

When a PMe_3 ligand replaces a CO the Mo dπ levels come closer together in energy in both mono- and di-nuclear species, and in the latter the out-of-phase $d_{x^2-z^2}$ and d_{xy} combinations

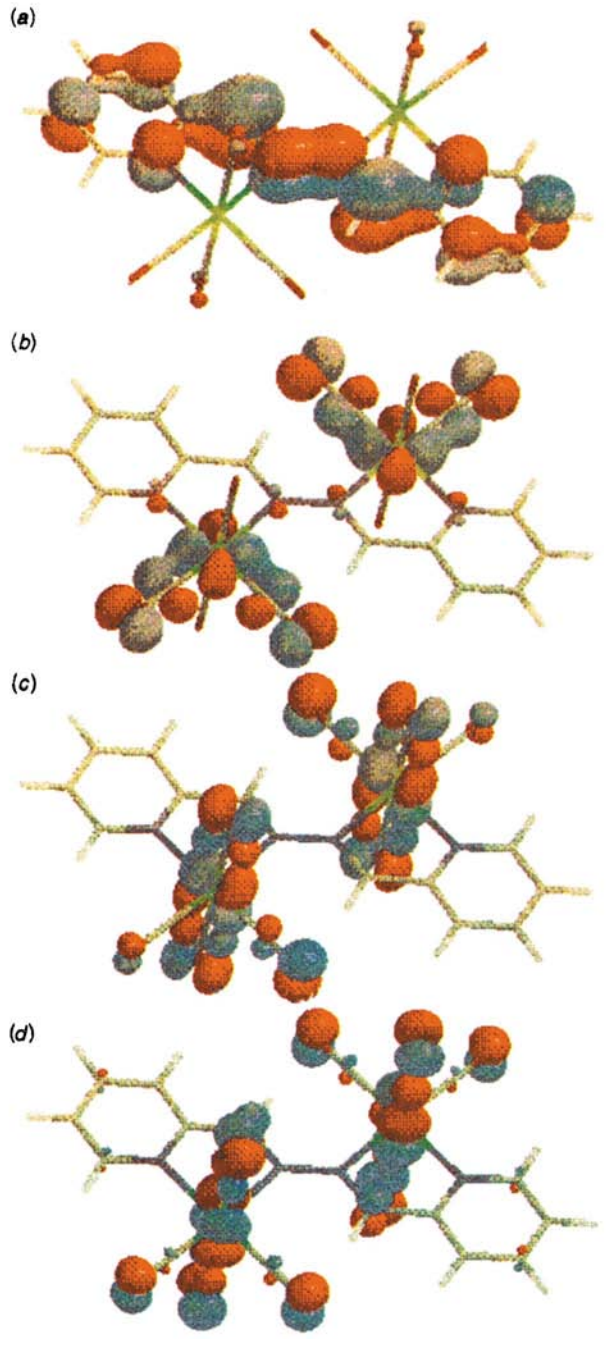

Fig. 2 Molecular orbital surfaces for the LUMO (*a*) and the in-phase Mo orbital combinations, HOMO (*b*), HOMO-3 (*c*) and HOMO-4 (*d*), for $[Mo_2(CO)_8(\mu\text{-pa})]$

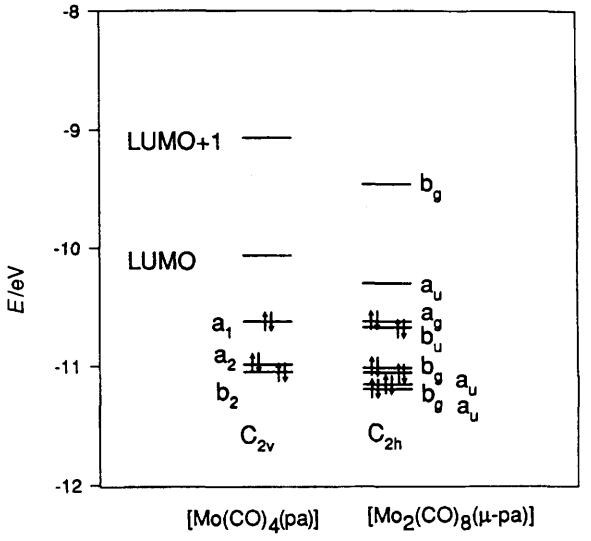

Fig. 3 Diagram showing orbital symmetries and calculated energies for the mononuclear and dinuclear $[Mo(CO)_4]$ complexes. The symmetry and the calculated ordering of energy levels differs slightly in the phosphine-substituted complexes; for C_i symmetry: LUMO + 1 (a_g), LUMO (a_u), HOMO (a_g, $d_{x^2-z^2}$), HOMO-1 and HOMO-3 ($2a_u$, mixed $d_{x^2-z^2}$ and d_{xy}), HOMO-2 (a_g, d_{xy}), HOMO-4 (a_g, d_{yz}), HOMO-5 (a_u, d_{yz})

mix due to the lowering of the symmetry. However this should have little effect on the electronic spectra since the transitions involving these orbitals are predicted to be very weak (see below).

The EHMO calculations show the LUMO and LUMO + 1 to be 5000–8000 cm^{-1} apart, depending on the coligands, dihedral angle and number of metals co-ordinated. The experimental differences are approximately 7000–9000 cm^{-1}, based on the differences between the peak positions of the two charge-transfer bands (see below). As mentioned above, since this latter is a difference between states it is only an approximation of the orbital energy difference. The calculated splitting decreases on phosphine-substitution, dinucleation and twisting about the centre of the pa ligand. The ordering of calculated energies of this gap agrees remarkably well with the observed order; $[Mo(CO)_4(pa)] \approx [Mo(CO)_3(PR_3)(pa)] > [Mo_2(CO)_8(\mu\text{-pa})] > [Mo_2(CO)_6(PR_3)_2(\mu\text{-pa})] > [Mo_2(CO)_6(\mu\text{-dppe})(\mu\text{-pa})]$, although the observed differences are smaller and less well defined because the higher energy charge-transfer band is only clearly observed in the two phosphine-substituted dinuclear complexes. The significant decrease in the LUMO–LUMO + 1 gap for the dinuclear species compared to the mononuclear complexes is probably due to the LUMO + 1 being more localised on the unmetallated half of the ligand so that it is not lowered in energy by the co-ordination of the metal as much as is the LUMO (note that the Mo carries a net positive charge even though it is formally Mo^0).

In $[Mo_2(CO)_7(PMe_3)(\mu\text{-pa})]$ the metal d orbitals are apparently sufficiently different in energy that they are effectively non-interacting. Each set has approximately the same energies as in the corresponding mononuclear species while the LUMO and LUMO + 1 energies are intermediate between those of the octacarbonyl dinuclear and the bis(PMe_3) analogue.

Electronic spectra

In common with other species of this type, all the new molybdenum pa complexes and the parent complex, $[Mo_2(CO)_8(\mu\text{-pa})]$,[6] show intense, solvatochromic absorptions in the visible region (Table 5, Fig. 4). These are assigned to metal-to-ligand charge-transfer (m.l.c.t.) transitions from the Mo 't_{2g}' orbitals to the pa ligand π^* system (LUMO and LUMO + 1);[2–6,9a] they will be referred to as m.l.c.t. 1 and m.l.c.t. 2 respectively. Both bands are about 1000 cm^{-1} lower in energy in the dinuclear than in the mononuclear species for the tetracarbonyl and the phosphine-substituted complexes; the corresponding calculated *orbital* energy differences are about 600 and 1000 cm^{-1} for the PMe_3-substituted and tetracarbonyl species respectively. These shifts are much smaller than the > 3000 cm^{-1} shift which occurs in the bipyrimidine-bridged $[Mo(CO)_4]_2$ analogues.[3,5,9a] As a result of the lowering of the π^* levels both m.l.c.t. 1 and m.l.c.t. 2 can be observed in the visible region in the dinuclear species, whereas in the mononuclear analogues the m.l.c.t. 2 bands occur as shoulders which are most clearly seen in spectra obtained in solvents of low polarity and in the spectra of $[Mo(CO)_3(PPh_3)(pa)]$ (*e.g.* 417 nm in diethyl ether).

The m.l.c.t. bands in the phosphine derivatives are shifted to

Table 5 Electronic absorption maxima of the molybdenum pyridine-2-carbaldehyde azine complexes[a]

	m.l.c.t. 2/cm^{-1} (ε/dm^3 mol^{-1} cm^{-1})	f[b]	m.l.c.t. 1/cm^{-1} (ε/dm^3 mol^{-1} cm^{-1})	f[b]
$[Mo(CO)_4(pa)]$[c]			18 200 (4 400)	0.09
$[Mo_2(CO)_8(\mu\text{-pa})]$	25 000 (sh)		17 000 (6 300)	
$[Mo(CO)_3(PPh_3)(pa)]$	23 250 (sh)		15 600 (3 700)	0.08
$[Mo_2(CO)_6(PPh_3)_2(\mu\text{-pa})]$	21 800 (6 500)	0.12	14 400 (5 000)	0.15
$[Mo_2(CO)_6(\mu\text{-dppe})(\mu\text{-pa})]$	21 500 (4 900)	0.11	14 550 (6 500)	0.11
$[Mo_2(CO)_7(PPh_3)(\mu\text{-pa})]$	21 300 (sh)		16 450 (br), 13 900 (sh)	
	25 750,[d] 21 850[d]		17 800,[d] 14 500[d]	

[a] Data are for dichloromethane solutions except where noted; sh = shoulder, br = broad. ε values show little variation with solvent. [b] Experimental oscillator strengths were estimated from the equation,[38] $f = 4.6 \times 10^{-9}\ \varepsilon\ \Delta\nu_{\frac{1}{2}}$, where $\Delta\nu_{\frac{1}{2}}$ is the bandwidth at half height. For m.l.c.t. 2 the half bandwidth was estimated by doubling the width of the lower energy half of the band. [c] In diethyl ether m.l.c.t. 2 = 27 050 (sh) and m.l.c.t. 1 = 17 750 cm^{-1}. [d] Values obtained from Gaussian deconvolution of the spectrum in acetonitrile.

Table 6 Calculated oscillator strengths for molybdenum pyridine-2-carbaldehyde azine complexes

Transition[a]	Complex[b]					
	$[Mo(CO)_4$-(pa)]	$[Mo(CO)_3$-(PMe_3)(pa)]	$[Mo_2(CO)_8$-$(\mu$-pa)]	$[Mo_2(CO)_6$-$(PMe_3)_2(\mu$-pa)][c]	$[Mo_2(CO)_6(\mu$-dmpe)$(\mu$-pa)][d]	$[Mo_2(CO)_7$-$(PMe_3)(\mu$-pa)]
$d_{x^2-z^2} \longrightarrow pa(\pi_1^*)$	0.000	0.002	0.000	0.000	0.001	0.000[e]
			0.000	0.000	0.001	0.000[f]
$d_{xy} \longrightarrow pa(\pi_1^*)$	0.000	0.001	0.000	0.001	0.002	0.000[e]
			0.008	0.000	0.004	0.000[f]
$d_{yz} \longrightarrow pa(\pi_1^*)$	0.068	0.104	0.000	0.139	0.202	0.068[e]
			0.065	0.000	0.005	0.045[f]
m.l.c.t. 1 total	0.068	0.11	0.073	0.14	0.21	0.11
$d_{x^2-z^2} \longrightarrow pa(\pi_2^*)$	0.000	0.002	0.000	0.000	0.010	0.008[e]
			0.000	0.008	0.012	0.000[f]
$d_{xy} \longrightarrow pa(\pi_2^*)$	0.028	0.015	0.022	0.000	0.000	0.011[e]
			0.000	0.006	0.000	0.018[f]
$d_{yz} \longrightarrow pa(\pi_2^*)$	0.062	0.232	0.152	0.000	0.000	0.275[e]
			0.000	0.423	0.367	0.055[f]
m.l.c.t. 2 total	0.090	0.25	0.17	0.44	0.39	0.37

[a] For the dinuclear species the two rows of figures for each transition correspond to the transitions from the out-of-phase and in-phase combinations of the Mo d orbitals. [b] Dihedral angles at centre of pa ligand, C=N–N=C, are 180° unless otherwise noted. [c] C_i symmetry isomer (PMe_3 on opposite faces of complex). [d] Dihedral angle C=N–N=C = −141° as in crystal structure. [e] Transition from $[Mo(CO)_3(PMe_3)]$ group. [f] Transition from $[Mo(CO)_4]$ group.

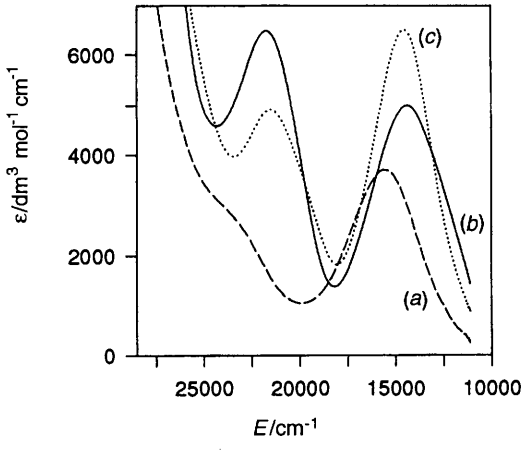

Fig. 4 Electronic spectra of (*a*) $[Mo(CO)_3(PPh_3)(pa)]$, (*b*) $[Mo_2(CO)_6(PPh_3)_2(\mu\text{-pa})]$ and (*c*) $[Mo_2(CO)_6(\mu\text{-dppe})(\mu\text{-pa})]$ in dichloromethane

the red compared to the parent tetracarbonyl species due to the destabilisation of the Mo 4d levels by the strongly donating phosphines.[4b,33] This shift, of 3000 cm^{-1}, is almost exactly equal to the calculated shift (based on orbital energy differences) for both pairs of complexes. The asymmetric dinuclear complex $[Mo_2(CO)_7(PPh_3)(\mu\text{-pa})]$ shows a complex spectrum as a result of the overlapping of the bands from the two distinct metal centres. Gaussian deconvolution of the spectrum in acetonitrile shows four strong bands, as predicted by the EHMO calculations (Table 6), in the region 350–900 nm (Table 5).

Oscillator strength calculations, while not expected to give accurate absolute numbers using this level of theory, should be reasonably reliable for giving relative intensities of transitions from the various d orbitals to the pa π* levels, although the experimental oscillator strengths will be affected by configuration interaction since the transitions are between states rather than orbitals. We have found good agreement between experimental data and values calculated by our program for a variety of complexes.[34,35] For the pa complexes (Table 6) we calculate that 69–99% of the intensity of m.l.c.t. 1 and m.l.c.t. 2 derives from transitions from the d_{yz} orbitals (the percentage is always lower for m.l.c.t. 2 than for m.l.c.t. 1 for planar complexes). Transitions from d_{xy} and $d_{x^2-z^2}$ are relatively very weak; the latter is σ to π in nature (overlap forbidden), whereas the former is formally allowed but weak perhaps because of poor overlap.[31,36,37]

In the mononuclear species m.l.c.t. 1 can be assigned to $Mo(d_{yz}) \longrightarrow pa(\pi_1^*)$, $b_2 \longrightarrow b_2^*$ in C_{2v} symmetry, and m.l.c.t. 2 is $Mo(d_{yz}) \longrightarrow pa(\pi_2^*)$, $b_2 \longrightarrow b_2^*$ in C_{2v}. In the tetracarbonyl dinuclear complexes with planar pa the real symmetry is C_{2h} and the LUMO and LUMO + 1 have a_u and b_g symmetry respectively. The metal orbital in- and out-of-phase combinations give symmetries as shown in Fig. 3. In the flat dinuclear species, as in the mononuclear, only one transition to each pa π* orbital is allowed, from the b_g d_{yz} combination to the a_u (LUMO) resulting in m.l.c.t. 1, and from the a_u d_{yz} combination to the b_g LUMO + 1, giving m.l.c.t. 2.

Table 7 Redox potentials for the molybdenum pyridine-2-carbaldehyde azine complexes

Compound	Potentials/V *vs.* SCE[a]	
	E_{ox}	E_{red}[b]
$[Mo(CO)_4(pa)]$	+0.84 (irr)	−0.85 (70), −1.58 (irr)
$[Mo_2(CO)_8(\mu\text{-pa})]$	*c*	−0.60 (70), −1.12 (70)
$[Mo(CO)_3(PPh_3)(pa)]$	+0.53 (irr)	−1.04 (70), −1.62 (irr)
$[Mo_2(CO)_6(PPh_3)_2(\mu\text{-pa})]$	+0.58 (irr)	−0.75 (60), −1.39 (irr)
$[Mo_2(CO)_6(\mu\text{-dppe})(\mu\text{-pa})]$	+0.61 (irr)	−0.78 (60), −1.29 (70)
$[Mo_2(CO)_7(PPh_3)(\mu\text{-pa})]$	+0.55 (irr)	−0.62 (60), −1.25 (irr)

[a] Data obtained from cyclic voltammograms recorded at 100 mV s^{-1} in dmf. [b] Peak to peak separations (mV) are given in parentheses. [c] Very broad peak.

Thus in the dinuclear species, unlike the mononuclear, the strong transitions originate from molecular orbitals that do not mix with the orbitals on which the transitions terminate.

The symmetry of the PMe_3 (PPh_3) dinuclear complexes is C_i if the phosphines are on opposite faces of the molecule, and C_2 if they are on the same face. None of our theoretical or experimental data can distinguish between these two possibilities; the calculated spectroscopic intensities are almost identical for the two cases, and give the same pattern of intensities as the C_{2h} case. Therefore the effective symmetry is higher than the actual symmetry, as is often the case,[38] and the determining factor in the 'allowedness' of the m.l.c.t. transitions is the parity, or g $\rightleftharpoons$ u nature, of the transitions *in the parent* C_{2h} *species*.

The dppe-bridged complex also has C_2 symmetry in spite of the 141° twist angle, and again the pattern of intensities is similar to that in the C_{2h} parent octacarbonyl complex except that there is more intensity in the $d_{xy} \longrightarrow pa(\pi^*)$ transitions. In all solvents, except Me_2SO and cyclohexanone, m.l.c.t. 1 lies at slightly higher energy in the dppe-bridged complex than in the bis(PPh_3) analogue (see SUP No. 57177). In contrast m.l.c.t. 2 is red shifted in the dppe-bridged species compared to the bis(PPh_3) analogue. This is the behaviour predicted by the calculations if the bis(PPh_3) complex has a planar pa ligand and the dppe species has a dihedral angle between 180 and 90° at the centre; (see above) the LUMO and LUMO + 1 become closer in energy as the dihedral angle becomes smaller whereas there is little effect on the metal orbitals.

Theoretical and experimental intensities

The theoretical oscillator strength or integrated intensity of a transition is calculated from equation (1). The term in

$$f = (8\pi^2 mc/3h)\,\bar{\nu}\,Q^2 \qquad (1)$$

parentheses is made up of constants (the symbols have their usual meanings), $\bar{\nu}$ is the energy of the transition, in m^{-1} if SI units are used for the constants, and Q is the transition dipole moment which we *estimate* using the extended-Hückel method with charge iteration. Thus, as mentioned above, the calculation is based on orbitals rather than states and the true f values will be affected by configuration interaction. The value of Q depends on the degree of overlap of the metal and ligand orbitals, and on the change in dipole moment between the ground and excited state, *i.e.* the degree of charge-transfer character.[38]

Experimental oscillator strengths were estimated for the visible region bands of four complexes (see Table 5). Remarkably good agreement is found between observed and calculated intensities for m.l.c.t. 1 in all complexes for which we have data. Calculated intensities for m.l.c.t. 2 are significantly higher than those observed (see below).

The presence of two m.l.c.t. bands of comparable intensity in the visible region, separated by at least 7500 cm^{-1}, for both mono- and di-nuclear species supports our assertion that the pa ligand is flat, or nearly so, in all species except the dppe-bridged complex where the separation of the two m.l.c.t. bands is smallest. Any twisting of pa away from planarity moves the two transitions closer together, as in the dppe-bridged species.

The bands in the dinuclear species have significantly larger oscillator strengths than the analogous bands in the mononuclear species. We have previously found similar behaviour for the corresponding bipyrimidine $[Mo(CO)_4]$ and $[W(CO)_4]$ complexes.†[9a] Our calculations predict slightly larger intensities for the dinuclear pa complexes compared to the mononuclear analogues, due to increases in the contributions of the $d_{xy} \longrightarrow pa(\pi_1^*)$ and $d_{yz} \longrightarrow pa(\pi_1^*)$ components. The reasons for this are not clear, but probably relate to better overlap in the dinuclear complexes. There are considerable differences between the composition of the orbitals from which the electron is excited in the mono- and di-nuclear species but there are corresponding differences in the nature of the LUMOs and the net change or degree of charge transfer is calculated to be essentially the same.

Some intensity difference between m.l.c.t. 1 and m.l.c.t. 2 in the dinuclear species is also predicted by the calculations, though the calculated difference is larger than that observed; m.l.c.t. 2 is calculated to be more intense than m.l.c.t. 1 due to increases in the intensities of both the $d_{yz} \longrightarrow pa(\pi^*)$ and $d_{xy} \longrightarrow pa(\pi^*)$ transitions. However, these results are distorted by the energy term in equation (1). Our EHMO with charge iteration results routinely give energy gaps between (occupied) metal and (unoccupied) ligand levels that are around 10 000 cm^{-1} too small. For low-energy transitions this error appears to fortuitously cancel an error in the estimation of the Q^2 term[34,35] whereas for higher energy transitions the calculated energy is *relatively* closer to the observed energy and the error is not cancelled completely. When the energy term is factored out the Q^2 values for m.l.c.t. 1 and m.l.c.t. 2 are very similar for both dinuclear phosphine-substituted complexes.

We have considered in detail the pattern of the m.l.c.t. bands in the two dinuclear phosphine-substituted complexes; while the overall intensities are similar for all four bands (m.l.c.t. 1 and 2 in both species) the half bandwidths vary considerably. However, based on the calculations (splitting of the d orbitals, pattern of intensities) we are unable to find a satisfactory explanation for the variation. In general the dppe-bridged species is predicted to have broader bands because relatively less of the intensity is concentrated in the main transitions.

Cyclic voltammetry

Electrochemical results for the pa complexes in dmf are presented in Table 7. In the range 0–1.0 V all the complexes exhibit irreversible oxidation waves; only the first peaks are listed. In contrast all complexes display a one-electron, reversible first reduction process, centred on the pa ligand.[6] The potentials of the dinuclear compounds, $[Mo_2(CO)_8(\mu\text{-pa})]$ and $[Mo_2(CO)_6(PPh_3)_2(\mu\text{-pa})]$ are shifted positively compared to their respective mononuclear species. Substitution of a carbonyl by a phosphine ligand causes small negative shifts in the pa reduction potentials and larger negative shifts in the (irreversible) oxidation potentials, correlating with the red shifts in the electronic spectra for both the mono- and di-nuclear species and with the EHMO results.

The asymmetric complex, $[Mo_2(CO)_7(PPh_3)(\mu\text{-pa})]$, is reduced at a potential between that of the octacarbonyl

† Previously we noted[9b] that the total m.l.c.t. 1 + m.l.c.t. 2 intensity for the dinuclear bipyrimidine complexes was double that of the mononuclear species. Our recent calculations suggest that this is fortuitous.

Table 8 Fits of the solvatochromism data to McRae's equation and correlations with Lees's E^*_{MLCT} parameter

	McRae parameters[a,b]				Lees parameters[a,c]		
Complex	$A + B$	C	E_{gas}	R	G	F	R
$[Mo(CO)_4(pa)]$	11 200	4 100	14 500	0.974	3 400	16 500	0.967
$[Mo(CO)_3(PPh_3)(pa)]$	1 900	3 300	13 600	0.925	2 300	14 100	0.988
$[Mo_2(CO)_8(\mu\text{-pa})]$					3 800	15 050	0.954
$[Mo_2(CO)_6(PPh_3)_2(\mu\text{-pa})]$							
m.l.c.t. 1	8 800	2 300	11 700	0.932	1 800	13 300	0.959
m.l.c.t. 2	2 900	2 200	20 200	0.934	1 720	20 700	0.995
$[Mo_2(CO)_6(\mu\text{-dppe})(\mu\text{-pa})]$							
m.l.c.t. 1	500	2 200	13 500	0.894	1 600	13 600	0.979
m.l.c.t. 2	200	2 100	20 600	0.881	1 700	20 500	0.972

[a] Data in cm^{-1}. [b] The standard errors are 3000, 300–400 and 150–300 cm^{-1} for the $A + B$, C and E_{gas} terms respectively, except for the second complex which has a standard error of 4500 cm^{-1} for $A + B$ and 450 cm^{-1} for C. [c] Standard errors are 60–300 cm^{-1} for the slope and 40–250 cm^{-1} for the constant.

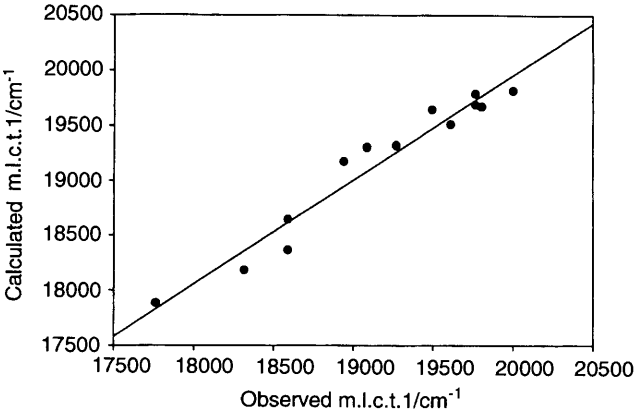

Fig. 5 Fit to McRae's equation for $[Mo(CO)_4(pa)]$

dinuclear and the bis(phosphine) species, but close to the value for the octacarbonyl complex, suggesting that the LUMO in the reduced species is not equally distributed over both ends of the pa ligand, in agreement with the calculations. The oxidation potential, albeit irreversible, is very close to that of $[Mo(CO)_3(PPh_3)(pa)]$, as predicted by the EHMO calculations (HOMO energies are similar). Similar behaviour occurs for the heterodinuclear $[(bipy)_2Ru(\mu\text{-bipym})Mo(CO)_4]^{2+}$ (bipy = 2,2′-bipyridine, bipym = 2,2′-bipyrimidine) complex; the reduction of the bipym ligand occurs at an average value of the homodinuclear analogues $[Ru_2(bipy)_4(\mu\text{-bipym})]^{4+}$ and $[Mo_2(CO)_8(\mu\text{-bipym})]$ while the metal centres, Ru and Mo, act independently.[5c]

The doubly bridged complex, $[Mo_2(CO)_6(\mu\text{-dppe})(\mu\text{-pa})]$, and the bis($PPh_3$) complex $[Mo_2(CO)_6(PPh_3)_2(\mu\text{-pa})]$ show quite similar redox behaviour, though the dppe-bridged species has a slightly more positive oxidation potential and a slightly more negative reduction potential, as predicted by the EHMO calculations which show that the LUMO is raised and the HOMO is lowered when the dihedral angle changes from 180 to −141° (due to less interaction between the two ends of the pa ligand). In the dppe-bridged complex both reductions are reversible; by contrast in the bis(PPh_3) complex only the first one is reversible, perhaps because the bridging dppe blocks a following reaction that occurs in the singly bridged bis(PPh_3) species.

Solvatochromism

Two methods were used to evaluate the solvatochromic behaviour of representative species (see Table 8 and SUP No. 57177): the method of Manuta and Lees[39] by using the empirical solvent parameter E^*_{MLCT}, and the more fundamental method of McRae,[40] based on the dielectric continuum model. Both methods proved reasonably successful, giving straight lines which reproduce most of the observed electronic spectroscopic peak positions to within about 200 cm^{-1} (*c.f.* experimental error of 50–80 cm^{-1}). In most cases the empirical parameter E^*_{MLCT} gives better correlations than McRae's equation, but it is less useful for elucidating the causes of the solvatochromism. A fit to McRae's equation for one complex is shown in Fig. 5.

The linear correlations with the Lees parameter can be expressed by equation (2), where E_{op} signifies the optical

$$E_{op} = F + GE^*_{MLCT} \quad (2)$$

charge-transfer energy (m.l.c.t. 1 or m.l.c.t. 2), and the sensitivity towards the solvent is given by the slope G. The slopes are lower for the phosphine-containing complexes than for the tetracarbonyl species, and, in the case of $[Mo_2(CO)_6(PPh_3)_2(\mu\text{-pa})]$ compared with $[Mo(CO)_3(PPh_3)(pa)]$, are lower for the dinuclear than the mononuclear species. These differences are probably due to increases in the amount of mixing of the metal and pa π* orbitals, and decreases in the amount of charge-transfer character, in the dinuclear species compared to the corresponding mononuclear species (due to lowering of the pa π* level) and in the phosphine complexes compared to the tetracarbonyls (due to raising of the Mo d orbital energies on phosphine substitution[36]). This explanation is supported by our calculations [we calculate more metal character to be in the LUMO in the dinuclear compared to the mononuclear species and more metal character in the LUMOs of the phosphine-substituted complexes compared to the carbonyls (Table 4)]. However, for the tetracarbonyl species, $[Mo(CO)_4(pa)]$ and $[Mo_2(CO)_8(\mu\text{-pa})]$, the difference in the slopes is fairly small and within experimental error.

The slopes for the two related dinuclear complexes, $[Mo_2(CO)_6(PPh_3)_2(\mu\text{-pa})]$ and $[Mo_2(CO)_6(\mu\text{-dppe})(\mu\text{-pa})]$, are the same within experimental error, indicating that the change in dihedral angle has no measurable effect on the interaction with the solvent. The solvatochromism of the asymmetric complex $[Mo_2(CO)_7(PPh_3)(\mu\text{-pa})]$ was not evaluated because of the difficulty in measuring the band energies with several overlapping bands.

McRae's equation uses dielectric continuum theory, assuming the solute to be a point dipole in a spherical cavity embedded in a dielectric continuum of the solvent,[40] *i.e.* it does not allow for ordering of the solvent around the solute molecules. Neglecting the Stark effect term, McRae's equation can be written as in equation (3), where E_{gas} is the charge

$$E_{op} = E_{gas} + (A + B)[(D_{op} - 1)/(2D_{op} + 1)] + C[(D_s - 1)/(D_s + 2) - (D_{op} - 1)/(D_{op} + 2)] \quad (3)$$

transfer energy in the gas phase, A, B and C are constants characteristic of the solute, D_{op} is the optical relative permittivity (square of the refractive index) and D_s is the static relative permittivity.

The first term (involving A) describes the contribution to the solvatochromism due to changes in dispersion forces. This term can be calculated [9b,40,41] and it is usually small and negative and can be neglected for highly polar species. The second (B) is the solute dipole–solvent induced dipole term which contributes if either the ground or excited state has a dipole moment. The third (C) is the dipole–dipole interaction term which can be non-zero only if the ground state effectively has a dipole moment. B and C can be expressed as in equations (4) and (5), where a is the effective cavity radius of the solute

$$B = (\mu_g^2 - \mu_e^2)/a^3 \quad (4)$$

$$C = 2\mu_g(\mu_g - \mu_e)/a^3 \quad (5)$$

and μ_g and μ_e are the ground and excited state dipole moments of the solute molecule, the latter referring to the *initally formed unequilibrated excited state*. If the first term is neglected μ_g and μ_e can, in principle, be calculated from a two parameter fit to the data. However, if B is larger than C imaginary results are obtained.

The McRae equation data show the contribution from dipole–dipole forces to be largest in the mononuclear $[Mo(CO)_4(pa)]$ complex, followed by $[Mo(CO)_3(PPh_3)(pa)]$ and then the dinuclear, phosphine-containing species. This ordering is similar to that obtained from the E^*_{MLCT} correlations.

As usual we have used only 'select solvents', as defined by Kamlet *et al.*,[42] for the McRae correlations because inclusion of chlorinated and aromatic solvents makes some of the correlations significantly worse and changes all of them. If a new line is defined which includes these solvents, they still give the largest differences between the calculated and observed values. It appears that the polarisability of these solvents is not adequately accounted for in McRae's treatment, or that higher order terms are important for these solvents.

The observation that the $(A + B)$ term is very large in the mononuclear species, $[Mo(CO)_4(pa)]$, is useful in that it demonstrates that this is not a feature specific to the dinuclear CO complexes as we thought previously.[9b] This is presumably an artefact due to the very 'sloppy' fit found for this term (see below).

The E^*_{MLCT} correlation also indicates that the solvatochromism is dominated by dipole–dipole interactions since recent work by Eisenberg and co-workers[43] showing correlations between the solvatochromism of platinum thiolate complexes (without carbonyl groups) and E^*_{MLCT} shows that this parameter does *not* describe specific solvent–solute interactions with the CO groups of the solute, or if it does it is only to the extent that these interactions are dipole–dipole in nature; we cannot distinguish experimentally between dipole–dipole interactions involving the molecular dipole and those involving individual bond dipoles and the solvent dipole.

The superior fit for the Lees parameter can be explained by the fact that it is an empirical parameter describing the dipole–dipole interactions, as well as weaker interactions, between solvent and solute *in a situation where the solvent is strongly ordered* {around $[Mo(CO)_4(bipy)]$ which has μ_g of about 10 D[31]}. The static and optical relative permittivities are bulk parameters which average the behaviour of the different parts of a solvent molecule. Thus, for a large solvent molecule containing a polar group and a hydrocarbon chain, the Lees parameter[39] should describe mainly the behaviour of the polar group, which is largely what the solute 'sees', whereas D_s and D_{op} describe an average property of the whole solvent molecule. Some support for this explanation comes from an analysis of the differences between observed and calculated transition energies which shows that the solvents containing the most C atoms or the longest hydrocarbon chains *tend* to have the largest deviations (however removing these solvents would change the correlation because there are few small, polar select[42] solvents, so this observation should be treated with caution).

This work provides further evidence that complexes which have no formal ground-state dipole moment interact with solvent as two individual polar halves. The various possibilities for the treatment of dinuclear species using McRae's equation have been discussed in an earlier publication.[9b] We conclude here from symmetry and the fact that the calculations indicate a small interaction between the two metal centres that the initial excited state is delocalised over both Mo centres as in a class III mixed-valence system.[44] In the time-scale of vibration(s) after the excitation it is likely that the complex relaxes to a localised state, formally Mo^0–pa^-–Mo^I, based on the work of Turner and co-workers,[45] using time-resolved infrared spectroscopy, on a related complex containing a weakly coupling bridging ligand (4,4′-bipyridine).

If this conclusion is correct, the angle between the two ground-state dipoles of the complex should not affect the solvatochromism, except for a slight modification of the sites available for interaction with the solvent, as we would conclude from the similar solvatochromism in the two different dinuclear complexes.

The solvatochromic behaviour of the mononuclear and dinuclear species is very similar in spite of (*i*) differences in the formal symmetry and the composition of the orbitals involved, (*ii*) the fact that approximately twice as many solvent molecules may interact with the dinuclear species compared to the mononuclear analogues, (*iii*) no formal permanent dipole moment in the planar dinuclear species, (*iv*) twice as many carbonyl groups being present in the dinuclear species, and (*v*) the orbital from which the electron moves being spread over two metals in the dinuclear species. McRae[40] has pointed out that the lack of a net dipole moment in the ground state will not result in the electric field (due to the ordering of the solvent molecules) being zero for a large molecule containing highly polar groups. The field due to the solvent around each half of the dinuclear complex will be similar to that around the corresponding mononuclear species if the overall electron distributions (net charges on the various atoms) are similar, and they are calculated to be quite similar.

The solvatochromism of highly polar complexes is largely determined by the magnitude of the ground-state dipole moment and thus the solvent stabilisation of the ground state, which is maximised in highly polar solvents with high D_s values. The composition of any given orbital (such as the one from which the electron is promoted) is not a factor in determining this interaction; it is the overall charge distribution that matters. The net movement of charge in the transition will, however, be a factor and we have shown this to be similar in related mono- and di-nuclear complexes (Table 4). This, as well as the electric field created by the solvent ordered around the ground state of the molecule, will determine the degree of destabilisation of the excited state, which will also vary with solvent.

In the dinuclear complexes there is movement of half a unit of charge from each end of the molecule, with each end being in an electric field equivalent to that in the mononuclear analogue. Summing the change over the two ends gives a pattern of change equivalent to the movement of one unit of charge from one Mo atom to pa in the mononuclear complex.

Conclusion

We have shown that EHMO theory with charge iteration is useful for understanding the properties of these Mo complexes. In combination with AM1 calculations the EHMO results have

shown the pa ligand to be planar except in the case where it is constrained by the presence of a second bridging ligand. Although the energy gaps between the occupied and unoccupied manifolds are not reproduced well (this is also the case for much higher levels of theory!) trends such as energy changes when ligands are changed are modelled extremely well. The theory has also been useful for gaining more detailed insights into the electrochemistry of the asymmetric dinuclear complex, and the electronic spectra and solvatochromic behaviour.

Acknowledgements

Financial support given by the Dirección de Investigación y Desarrollo de la Universidad de La Frontera (Project No. 9630), Fundación Andes (Estadia de Investigación) and the Natural Sciences and Engineering Research Council (Ottawa) to carry out this work is gratefully acknowledged.

References

1 P. J. Steel, *Coord. Chem. Rev.*, 1990, **106**, 227; V. Balzani and F. Scandola, *Supramolecular Photochemistry*, Ellis Horwood, New York, 1991, ch. 6; F. Scandola, M. T. Indelli, C. Chiorboli and C. A. Bignozzi, *Top. Curr. Chem.*, 1990, **158**, 73.
2 D. Walther, *Z. Anorg. Allg. Chem.*, 1973, **396**, 46; R. R. Ruminski and J. O. Johnson, *Inorg. Chem.*, 1987, **26**, 210; R. R. Ruminski and I. Wallace, *Polyhedron*, 1987, **8**, 1673; M. Shoup, B. Hall and R. R. Ruminski, *Inorg. Chem.*, 1988, **27**, 200; R. R. Ruminski, C. DeGroff and S. J. Smith, *Inorg. Chem.*, 1992, **31**, 3325; J. Granifo, *Polyhedron*, 1994, **13**, 713.
3 C. Overton and J. A. Connor, *Polyhedron*, 1982, **1**, 53; K. J. Moore and J. D. Petersen, *Polyhedron*, 1983, **2**, 279.
4 (*a*) S. Kohlmann, S. Ernst and W. Kaim, *Angew. Chem., Int. Ed. Engl.*, 1985, **24**, 684; (*b*) S. Ernst and W. Kaim, *Inorg. Chim. Acta*, 1988, **144**, 223; (*c*) W. Kaim, S. Ernst and S. Kohlmann, *Polyhedron*, 1986, **5**, 445.
5 (*a*) W. Kaim and S. Kohlmann, *Inorg. Chem.*, 1986, **25**, 3306; (*b*) W. Kaim and S. Kohlmann, *Inorg. Chem.*, 1987, **26**, 68; (*c*) W. Matheis and W. Kaim, *Inorg. Chim. Acta*, 1991, **181**, 15; (*d*) W. Kaim, S. Kohlmann, A. J. Lees, T. L. Snoeck, D. J. Stufkens and M. M. Zulu, *Inorg. Chim. Acta*, 1993, **210**, 159; (*e*) W. Kaim, W. Bruns, S. Kohlmann and M. Krejcik, *Inorg. Chim. Acta*, 1995, **229**, 143.
6 M. Haga and K. Koizumi, *Inorg. Chim. Acta*, 1985, **104**, 47.
7 K. Kalyanasundaram and M. Nazeeruddin, *J. Chem. Soc., Dalton Trans.*, 1990, 1657; J. W. M. van Outersderp, D. J. Stufkens and A. Vlcek, Jr., *Inorg. Chem.*, 1995, **34**, 5183, and refs. therein.
8 W. Kaim and V. Kasack, *Inorg. Chem.*, 1990, **29**, 4696.
9 (*a*) E. S. Dodsworth and A. B. P. Lever, *Coord. Chem. Rev.*, 1990, **97**, 271; (*b*) *Inorg. Chem.*, 1990, **29**, 499.
10 D. M. Manuta and A. J. Lees, *Inorg. Chem.*, 1986, **25**, 3212; M. M. Zulu and A. J. Lees, *Inorg. Chem.*, 1988, **27**, 3325.
11 W. Kaim, S. Kohlmann, S. Ernst, B. Olbrich-Deussner, C. Bessenbacher and A. Schulz, *J. Organomet. Chem.*, 1987, **321**, 215.
12 D. J. Stufkens, *Coord. Chem. Rev.*, 1990, **104**, 39.
13 W. J. Stratton and D. H. Busch, *J. Am. Chem. Soc.*, 1958, **80**, 1286.
14 D. J. Darensbourg and R. L. Kump, *Inorg. Chem.*, 1978, **17**, 2680.
15 P. Correa, M. E. Vargas and J. Granifo, *Polyhedron*, 1987, **6**, 1781.
16 S. Sahami and M. J. Weaver, *J. Electroanal. Chem.*, 1981, **122**, 171.
17 J. Baker, *J. Comput. Chem.*, 1992, **13**, 240.
18 R. A. Metcalfe, E. S. Dodsworth, A. B. P. Lever, W. J. Pietro and D. J. Stufkens, *Inorg. Chem.*, 1993, **32**, 3581.
19 R. J. Hoffmann, *J. Chem. Phys.*, 1963, **39**, 1397; H. Basch, A. Viste and H. B. Gray, *J. Chem. Phys.*, 1966, **44**, 10.
20 G. Calzaferri and R. Rytz, *J. Phys. Chem.*, 1995, **99**, 12141.
21 S. S. Fielder, A. B. P. Lever and W. J. Pietro, unpublished work.
22 A. Vela and J. L. Gazquez, *J. Phys. Chem.*, 1988, **92**, 5688.
23 N. Walker and D. Stuart, *Acta Crystallogr., Sect. A*, 1983, **39**, 158.
24 G. M. Sheldrick, SHELX 76, Program for Crystal Structure Determination, University of Cambridge, 1976; SHELXS 86, Program for Crystal Structure Determination, University of Göttingen, 1986.
25 A. Griffiths, *J. Cryst. Mol. Struct.*, 1971, **1**, 75; K.-B. Shiu, S.-L. Wang and F.-L. Liao, *J. Organomet. Chem.*, 1991, **420**, 207; W. Kaim, S. Kohlmann, J. Jordanov and D. Fenske, *Z. Anorg. Allg. Chem.*, 1991, **598,599**, 217.
26 K. K. Cheung, T. F. Lai and K. S. Mok, *J. Chem. Soc. A*, 1971, 1644; I. Bernard, G. M. Reisner, G. R. Dobson and C. B. Dobson, *Inorg. Chim. Acta*, 1986, **121**, 199; C. H. Veng and G. Y. Hwang, *Acta Crystallogr., Sect. C*, 1991, **47**, 522; C. H. Veng and G. Y. Hwang, *Inorg. Chim. Acta*, 1994, **218**, 9.
27 F. H. Allen and O. Kennard, *Chemical Design Automation News*, 1993, **8**, 31.
28 A. G. Orpen, L. Brammer, F. H. Allen, O. Kennard, D. G. Watson and R. Taylor, *J. Chem. Soc., Dalton Trans.*, 1989, S1.
29 M. H. B. Stiddard, *J. Chem. Soc.*, 1962, 4712; C. S. Kraihanzel and F. A. Cotton, *Inorg. Chem.*, 1963, **2**, 533.
30 L. W. Houk and G. R. Dobson, *Inorg. Chem.*, 1966, **5**, 2119.
31 R. W. Balk, D. J. Stufkens and A. Oskam, *Inorg. Chim. Acta*, 1978, **28**, 133.
32 Y.-G. K. Shin, B. S. Brunschwig, C. Creutz, M. D. Newton and N. Sutin, *J. Phys. Chem.*, 1996, **100**, 1104.
33 H. tom Dieck and I. W. Renk, *Angew. Chem., Int. Ed. Engl.*, 1970, **9**, 793.
34 A. DelMedico, E. S. Dodsworth, S. S. Fielder, A. B. P. Lever and W. J. Pietro, unpublished work.
35 R. A. Metcalfe, E. S. Dodsworth, S. S. Fielder, D. J. Stufkens, A. B. P. Lever and W. J. Pietro, *Inorg. Chem.*, in the press.
36 H. tom Dieck and I. W. Renk, *Chem. Ber.*, 1971, **104**, 110; H. tom Dieck and I. W. Renk, *Chem. Ber.*, 1972, **105**, 1403.
37 L. H. Staal, D. J. Stufkens and A. Oskam, *Inorg. Chim. Acta*, 1978, **26**, 255.
38 A. B. P. Lever, *Inorganic Electronic Spectroscopy*, 2nd edn. Elsevier, Amsterdam, 1984.
39 D. M. Manuta and A. J. Lees, *Inorg. Chem.*, 1983, **22**, 3825.
40 E. G. McRae, *J. Phys. Chem.*, 1957, **61**, 562.
41 N. S. Bayliss, *J. Chem. Phys.*, 1956, **18**, 292.
42 M. J. Kamlet, J.-L. M. Abboud and R. W. Taft, *Prog. Phys. Org. Chem.*, 1981, **13**, 485.
43 J. M. Bevilacqua and R. Eisenberg, *Inorg. Chem.*, 1994, **33**, 2913; S. D. Cummings and R. Eisenberg, *Inorg. Chem.*, 1995, **34**, 2007.
44 M. B. Robin and P. Day, *Adv. Inorg. Chem. Radiochem.*, 1967, **10**, 248.
45 M. W. George, J. J. Turner and J. R. Westwell, *J. Chem. Soc., Dalton Trans.*, 1994, 2217.

Received 25*th June* 1996; *Paper* 6/04437I